Measurements of temporally modulated LED light sources

Ville Mantela

Aalto University

Aalto University publication series
Doctoral Theses 164/2025

Measurements of temporally modulated LED light sources

Ville Mantela

A doctoral thesis completed for the degree of Doctor of Science (Technology) to be defended, with the permission of the Aalto University School of Electrical Engineering, at a public examination held at the lecture hall TU1, Maarintie 8, on 19 September 2025 at 12:00.

Aalto University
School of Electrical Engineering
Department of Electrical Engineering and Automation
Metrology Research Institute

Supervisor
Prof. Erkki Ikonen, Aalto University, Finland

Thesis advisors
D.Sc. (Tech.) Petri Kärhä, Aalto University, Finland

Preliminary examiners
Dr. Carsten Dam-Hansen, Technical University of Denmark, Denmark
Prof. Markku Kuittinen, University of Eastern Finland, Finland

Opponent
Dr. Carsten Dam-Hansen, Technical University of Denmark, Denmark

Aalto University publication series
Doctoral Theses 164/2025

ISBN 978-952-64-2699-0 (paperback)
ISBN 978-952-64-2698-3 (PDF)
ISSN 1799-4934 (printed)
ISSN 1799-4942 (PDF)

http://urn.fi/URN:ISBN:978-952-64-2698-3

Unigrafia Oy
Helsinki 2025

Aalto University

ABSTRACT

Author Ville Mantela

Name of the doctoral thesis Measurements of temporally modulated LED light sources

Article-based thesis

Number of pages 32

Keywords Flicker, Stroboscopic effect, LED light sources

LED-based light sources have become the *de facto* light source type in recent years due to having superior energy efficiency when compared to traditional incandescent light sources, along with regulations made worldwide banning the sales of incandescent, fluorescent, compact fluorescent and mercury based light sources to consumers. This shift in lighting technology has created challenges in optical metrology, especially as the LED sources have different temporal modulation characteristics to incandescent light sources.

Temporal Light Modulation (TLM) is the variation in illumination over time, which can cause different ill effects on human health under the illumination of these sources, ranging from annoyance to even epileptic seizures. The LED differs from incandescent sources in temporal behaviour as the diodes only work on direct current (DC), while incandescent light sources use the alternating current (AC) coming from the electric source, such as electrical outlet at homes. The electronics needed to the AC-DC conversion affects the temporal behaviour of the LED lights, resulting in various temporal light outputs.

In this thesis, advancements in the measurements of temporally modulated light~~s~~ are demonstrated. First, a novel set of Temporal Light Artefact (TLA) software was created to calculate the metrics of temporally modulated light more accurately than previously available methods. Secondly, a hyperspectral camera-based measurement method was tested to enable the measurement of more complex LED arrangements, including multiple sources, and measurement of TLA from different parts of spectrum. Finally, the Ecodesign regulation in the European Union, which sets limits for TLA parameters in consumer-grade LED light sources, was addressed by measuring LED lamps that were manufactured both before and after the regulation was implemented. It was found that the regulation was considered by the manufacturers, and lamp types with lower TLA values were adopted, thereby minimizing the risk of adverse effects to humans.

Tekijä Ville Mantela

Väitöskirjan nimi Aikamoduloitujen LED-valonlähteiden mittauksia

Artikkeliväitöskirja

Sivumäärä 32

Avainsanat Välkyntä, Stroboskooppi-ilmiö, LED valonlähteet

LED-pohjaisista valonlähteistä on tullut vakiintunut valonlähdetyyppi viime vuosina, koska ne ovat energiatehokkaampia verrattuna perinteisiin hehkulamppuihin ja koska hehkulamppujen, sekä pienikokoisten energiansäästölamppujen ja elohopeaa sisältävien lamppujen myynti kuluttajille on kielletty maailmanlaajuisesti. Tämä valaistusteknologian muutos on aiheuttanut haasteita optisessa mittaustekniikassa, erityisesti koska LED-valonlähteillä on erilaiset aikamodulaatio-ominaisuudet verrattuna hehkulamppuihin.

Valon aikamodulaatio tarkoittaa valaistusvoimakkuuden vaihtelua ajan suhteen, mikä voi aiheuttaa erilaisia haittavaikutuksia niiden ihmisten terveydelle, jotka oleskelevat tällaisten valonlähteiden vaikutuspiirissä. Nämä haittavaikutukset voivat aiheuttaa oireita ärsytyksestä jopa epileptisiin kohtauksiin. LED-valot eroavat hehkulampuista aikamodulaationsa suhteen, sillä diodit toimivat ainoastaan tasavirralla (DC), kun taas hehkulamput käyttävät vaihtovirtaa (AC), jota tulee esimerkiksi kodin pistorasiasta. Tarvittava elektroniikka vaihtovirran muuntamiseen tasavirraksi vaikuttaa LED-valojen ajalliseen käyttäytymiseen ja aiheuttaa erilaisia valon aikamodulaatioita.

Tässä väitöskirjassa kehitetään ajallisesti moduloitujen valonlähteiden mittauksia. Aluksi kehitettiin uusi ohjelmistokokonaisuus aikamoduloidun valon suureiden (Temporal Light Artefact, TLA) laskemiseen, jonka avulla mittausten tarkkuutta pystyttiin parantamaan aiempiin menetelmiin verrattuna. Seuraavaksi testattiin hyperspektrikameraan perustuvaa mittausmenetelmää, jonka avulla pyrittiin mahdollistamaan monimutkaisempien, useita LED-valonlähteitä sisältävien järjestelmien mittaaminen, sekä mahdollistaa TLA-mittaukset eri kohdista valon spektriä. Lopuksi tutkittiin Euroopan unionin Ecodesign-asetuksen vaikutusta, jossa määritettiin rajoja kuluttajaluokan LED-valonlähteiden TLA-arvoille. Mittaamalla ennen ja jälkeen asetuksen voimaantuloa valmistettuja LED-lamppuja havaittiin, että valmistuksessa oli otettu huomioon asetuksen rajat ja siirrytty lampputyyppeihin, joissa TLA-arvot ovat alhaisemmat, mikä vähentää haitallisten vaikutusten riskiä ihmisille.

Preface

This research was carried out in Metrology Research Institute of Aalto University during the years 2020-2025. The work and publications for this thesis were produced for the scope of EURAMET EMPIR project MetTLM, *Metrology for Temporal Light Modulation*.

I am deeply grateful for Prof. Erkki Ikonen for the opportunity to work in this research group, hiring me during the difficult times of 2020, during the pandemic. The work in this group has been fulfilling, and I have learned a lot, both in knowledge and of myself. I am also grateful for Doc. Petri Kärhä, for his guidance and comments during my work, publications and in this thesis. I also would like to thank Dr. Carsten Dam-Hansen and Prof. Markku Kuittinen for their work as pre-examiners towards this thesis, your contribution has been crucial to the final form of this thesis.

I would like to give a huge thanks to the colleagues in the group, both current and previous. I have warm memories of all the times in the office, laboratories, coffee, lunch, and outside of work. I would like to name Dr. Janne Askola, as the person who taught me everything as I arrived at the group and taught me the skills I needed to continue my work. I am deeply indebted to everything you have done. I would also like to thank Roope Nordlund for his work contributing to the TLA codes and measurements. And similarly, Iiro Harju, contributing to the hyperspectral measurement setup. Thank you for your contributions.

Last, but not least, I would like to thank my family and friends who have been part of my journey during these last five years. Especially to my wife Hanna, who has been there for me during the ups and downs of my journey, supporting me through the difficult times, like the last few months while I have been busy finishing this thesis. And both of my little rascals, Benjamin and Max, for grounding me after workdays, keeping me busy during the weekends with your hobbies and curiosities, and making me laugh at your shenanigans.

Kellokoski, 18.8.2025

Ville W. Mantela

Contents

List of Publications

This doctoral dissertation consists of a summary and of the following publications by the author, which are referred to in the text by their numerals 1-3.

1. Mantela Ville, Nordlund Roope, Askola Janne, Kärhä Petri, Ikonen Erkki. Digital implementations for determination of temporal light artefacts of LED luminaires. *Lighting Research & Technology*. 2024;56(7):734-743. doi:10.1177/14771535231212404

2. Mantela Ville, Harju Iiro, Kärhä Petri, Ikonen Erkki. Measurement of temporal light artefacts using a hyperspectral camera, 6 pages, Submitted May 2025.

3. Mantela Ville, Nordlund Roope, Askola Janne, Kärhä Petri, Dekker Paul, Ikonen Erkki. Improvement of temporal light artefact effects in commercial LED lamps. *Lighting Research & Technology*. 2024;56(7):790-799. doi:10.1177/14771535241287549

Author's Contribution

1. “Digital implementations for determination of temporal light artefacts of LED luminaires”

The author was Aalto’s key contact in the MetTLM project and involved in developing a novel set of digital software implementations in MATLAB to overcome the limitations in the state-of-the-art implementations. His contribution was crucial in improving the software performance for final implementations. The author prepared the manuscript and modified it according to the comments received from the co-authors and referees.

2. “Measurement of temporal light artefacts using a hyperspectral camera.”

The author created a measurement setup to measure multiple light sources temporally with a hyperspectral camera to assess the spectral contributions of the temporal light modulation in the sources. He carried out the measurements and analysed the results. The author wrote the original manuscript and revised it according to the feedback from the co-authors.

3. “Improvement of temporal light artefact effects in commercial LED lamps”

The author arranged the measurement of 80 different types of commercial E27 based consumer LED lamps to test the effects of the European Union Ecodesign regulation that was set in 2021 to battle the flicker and stroboscopic effect of consumer lamps. He carried out the analysis of the TLA data of the sources, and comparisons to European Union database EPREL. The author drafted the manuscript and revised it by co-authors’ and referees’ comments.

List of Abbreviations

AC	Alternating current
ADC	Analog-to-digital converter
BIPM	The Bureau International des Poids et Mesures
CIE	Commission internationale l'éclairage, The International Commission on Illumination
CDF	Cumulative distribution function
CVC	Current-to-voltage converter
DC	Direct current
DFT	Discrete Fourier transform
CFL	Compact Fluorescent Lamp
DUT	Device under test
EMI	Electromagnetic interference
EMPIR	European Metrology Programme for Innovation and Research
EPREL	European Product Registry for Energy Labelling
ETS	Equivalent time sampling
EU	European Union
EURAMET	European Association of National Metrology Institutes
FFT	Fast Fourier Transform
fov	Field of view
fps	Frames per second
IEC	International Electrotechnical Commission
LED	Light Emitting Diode
MetTLM	Metrology for Temporal Light Modulation project
NMI	National Metrology Institute

RGB	Red, Green, Blue
SI	The International system of units
SVM	Stroboscopic effect visibility measure
TLA	Temporal Light Artefact
TLM	Temporal Light Modulation

List of Symbols

$C(f)$	Frequency spectrum
d_{E}	Peak-to-peak amplitude
E_{v}	Illuminance
$E(t)$	Illuminance waveform
F_{HP}	High-pass filter in Block B of the flickermeter
F_{LP}	Low-pass filter in Block C of the flickermeter
F_{LPBW}	6$^{\mathrm{th}}$ order low-pass Butterworth filter
$F_{\mathrm{WF}}^{\mathrm{LM}}$	Bandpass filter in Block B of the flickermeter
f_{c}	Cut-off frequency
f_{HP}	Cut-off frequency for the high-pass filter
f_{m}	Modulation frequency
f_{s}	Sampling frequency
I_v	Luminous intensity
j	Imaginary constant
K_{cd}	Luminous constant, 683 lm/W
M_{vs}	Stroboscopic effect visibility measure
N_{s}	Number of samples
P_{inst}	Instantaneous flicker sensation
P_q	Values of P_{inst} over q % probability
$P_{\mathrm{st}}^{\mathrm{LM}}$	Short-term flicker severity index
S_0	Scaling factor
$S(0)$	DC component of the frequency spectrum
$S(f)$	Two-sided frequency spectrum

s	Laplacian variable
$T(f)$	Visibility threshold function
T_{m}	Acquisition time
T_{s}	Sampling time
$u_{\mathrm{E}}(t)$	Input light waveform for flickermeter and SVM meter
$V(\lambda)$	Photopic sensitivity curve by CIE
w_{Hanning}	Hanning window
z	Complex Z-domain variable
τ_{HP}	Time constant for high-pass filter in Blcok B of flickermeter
τ_{LP}	Time constant of low-pass filter in Block C of flickermeter
Φ_{v}	Luminous flux
ω	angular frequency
ω_{m}	angular frequency from modulation frequency

1 Introduction

The incandescent light bulb, the original form of electric lighting, was developed in the late 19th century by multiple inventors, though it is most commonly credited to Thomas Edison, who patented a carbon filament bulb on January 27, 1880, in the United States [1]. This technology evolved over time and remained the dominant source of electric lighting until the early 21st century. The turning point came in the late 20th century with the invention of the blue light-emitting diode (LED) by Shuji Nakamura [2], alongside parallel developments by Isamu Akasaki and Hiroshi Amano [3]. Their breakthrough enabled the creation of white LED lighting and earned them the Nobel Prize in Physics in 2014 [4].

As the 21st century began, the European Union (EU) sought to reduce energy consumption across the continent. The emergence of energy-efficient alternatives such as compact fluorescent lamps (CFLs) and LEDs led to regulatory action in 2009 to phase out incandescent bulbs [5], culminating in a full sales ban in 2012 [6–8]. With higher durability and luminous efficacy, LED technology soon became the standard for lighting.

The widespread adoption of LEDs required industry and standardization bodies to adjust, as existing standards had been designed around the relatively simple incandescent bulbs. Incandescent lamps, essentially resistive wires driven by alternating current (AC), have luminous output directly proportional to the input current. In contrast, LEDs operate on direct current (DC) and require circuitry to convert mains AC to DC, introducing variability in luminous behaviour depending on the circuit design [9].

Most commercially available LED lamps are powered by AC, resulting in fluctuations in luminous output—known as temporal light modulation (TLM) [9,10]. These modulations can lead to temporal light artefacts (TLAs), which are the visible effects of TLM. TLAs include flicker, the stroboscopic effect, and the phantom array effect. TLAs are associated with a range of human health effects, from minor discomfort like headaches and eye strain to severe conditions such as epileptic seizures [9,11,12].

Flicker refers to noticeable changes or fluctuations in light luminance or spectral distribution that can be seen when both the viewer and the surroundings are still [10], commonly described as “flickering lights.” The stroboscopic effect is observed, for example, when rotating objects look like they are slowing down or even going backward because of

modulated lighting [10]. The phantom array effect, or "ghosting," happens when the eye moves rapidly from side to side (during a saccade) across a high contrast, modulated light source, causing it to appear as multiple points due to different parts of the retina being stimulated [10].

For flicker and stroboscopic effect, there are well established parameters, short-term flicker severity index $P_{\mathrm{st}}^{\mathrm{LM}}$ for flicker and stroboscopic effect visibility measure M_{vs} for stroboscopic effect, that are used to measure the severity of these effects to an average human observer [9, 10, 13]. Flicker describes TLAs in the frequency range of $0.1 - 80$ Hz, while M_{vs} is defined up to 2 kHz [13, 14]. The stroboscopic effect visibility measure is often referred by the abbreviation SVM in literature, but in this thesis symbol M_{vs} is used. Phantom array effect has not had a metric until April of 2024, when a metric was proposed by Tan et. al. [15]. In 2019, the EU Ecodesign regulation set limits for the flicker and stroboscopic effect in commercial household lamps [16]. The limit for flicker was set to $P_{\mathrm{st}}^{\mathrm{LM}} < 1$, which means that on average, this effect is not visible. For the stroboscopic effect, the limit was set initially to $M_{\mathrm{vs}} < 0.9$, and then lowered to $M_{\mathrm{vs}} < 0.4$ in September 2024. For the phantom array effect there is no standardized metric nor regulation at the time of writing.

1.1 Thesis outline

Chapter 2 of the thesis describes the implementations and measurement methods of temporally modulated light, both in practical measurement of TLM sources, used for Publications 2 and 3, and the digital implementations, described in Publication 1, used to calculate the TLA parameters from the measured light waveforms.

In Chapter 3, the effect of the 2019 EU Ecodesign regulation, related to TLA parameters, on consumer-grade LED sources is discussed based on the results of Publication 3 while using the implementations of Publication 1 in practice. The comparison between pre-regulation and post-regulation lamps will be presented and as well as discussion on manufacturers taking responsibility for their products complying to these regulations. The thesis is summarized in Chapter 4.

1.2 Scientific contribution

The thesis contains the following scientific contributions:

Publication 1. It was discovered that the earlier digital implementations for calculating $P_{\mathrm{st}}^{\mathrm{LM}}$ and M_{vs} values had inaccuracies with a set of known test waveforms. We developed

more accurate implementations in MATLAB software platform which reduced the deviations for the test waveform values given in the related standards. The Aalto flickermeter implementation decreased the calculation error of $P_{\mathrm{st}}^{\mathrm{LM}}$ by an order of magnitude, and the Aalto SVM meter decreased the average error of M_{vs} by almost two orders of magnitude. These implementations have been made publicly available in GitHub [17] during the publishing process, so anyone can use them for calculating the TLA parameters from waveforms.

Publication 2. In this publication we created a method to measure multiple light sources simultaneously for their TLM waveforms by utilizing a hyperspectral camera. The benefit of using a hyperspectral camera instead of regular camera is to be able to measure multiple sources simultaneously and get the temporal waveforms of spectral regions down to widths of about 10 nm. This would allow TLA measurements of multi-coloured light sources to assess the main contributor of TLA in the lamp.

Publication 3. We created a luminous flux-based measurement setup for measuring TLA parameters from commercial E27-based LED bulbs. With this setup we measured 80 different commercial LED lamps of which 60 lamp types were purchased in the EU market before the 2019 Ecodesign regulation, and 20 were purchased after the regulation. We found out that we could divide the lamps by the electrical circuitry into four main groups of circuit topologies, which have distinct temporal electrical and luminous fingerprints. With this information we could see if any changes in AC to DC conversion has appeared after the regulation was set. We found that the manufacturers have made changes in the light source electronics, they have stopped using the old circuit topologies that had significantly higher M_{vs} and have started to prefer a certain topology, which has $M_{\mathrm{vs}} \approx 0$.

2 Implementation of Temporal Light Artefact measurements

The measurement of TLAs have two phases, the physical measurement of light waveforms, and calculating the TLA parameters out of the waveform with appropriate software. In this chapter, we discuss first the digital implementations for calculation of TLA metrics, and what was done to improve these implementations in Publication 1. Then, the practical measurements of the light waveforms, which were used in Publications 2 and 3 are discussed in chapter 2.2.

2.1 Digital implementations for Temporal Light Artefacts

For light waveform calculations, digital TLA meters are used. IEC recommends in their technical reports [18] and [19] using MATLAB implementations that can be found in MATLAB software center [20]. The software was tested with the test waveforms given by IEC [17,18], but the result gave deviations of over 3 % from the expected value in flickermeter and over 2 % in stroboscopic effect visibility meter. Although these values fit into the allowed deviations of 5 % stated in the technical reports [18, 19], these errors are large for a software used to calculate the TLA parameters from the measured waveforms. After further testing, we decided to create our own implementations described in Publication 1. Early research to solve the issues with the IEC recommended implementations were also reported by Mantela et al. [21], Koch and Zuber [22] and Dam-Hansen et al. [23].

2.1.1 Flickermeter

Light flickermeter is an instrument for measurement of flicker in the scene [18]. The light flickermeter consists of four defined blocks A-D as shown in Figure 1. It takes the measured or simulated light waveform $u_{\mathrm{E}}(t)$ as the input parameter. The first block, Block A, works as the input adapter, i.e. it normalizes the light waveform by dividing it by the mean value. This allows determination of flicker regardless of the light level measured originally.

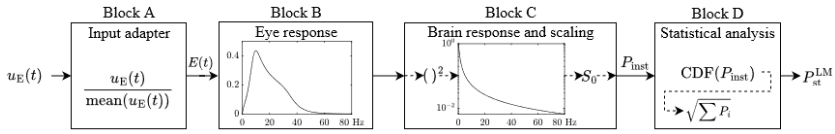

Figure 1. The block diagram of light flickermeter (from Publication 1).

In Block B, the normalized light waveform from Block A gets filtered by three different filters to mimic the human eye response to temporally modulated light. This is achieved using three different weighing filters. First, we remove the DC component from the signal with a 1st order high-pass filter with a cutoff frequency $f_{\mathrm{HP}} = 0.05$ Hz. The analogue filter transfer function for this filter is

$$F_{\mathrm{HP}}(s) = \frac{\tau_{\mathrm{HP}} \cdot s}{\tau_{\mathrm{HP}} \cdot s + 1}, \tag{1}$$

where $\tau_{\mathrm{HP}} = \frac{1}{2\pi \cdot f_{\mathrm{HP}}}$. For $f_{\mathrm{HP}} = 0.05$ Hz, we get $\tau_{\mathrm{HP}} = 3.183$ s. In Equation (1), $s = \omega j$ is the Laplace variable, where $\omega = 2\pi f_{\mathrm{m}}$ for modulation frequency f_{m}, and j is the imaginary constant. [18, 24-26].

The second filter in Block B is a 6th order low-pass Butterworth analogue filter with a cutoff frequency of 35 Hz for light sources under AC mains with 50 Hz frequency. This filter was selected as it has the flattest response in this passband. The 6th order Butterworth filter produces -50 dB attenuation at 100 Hz mains frequency [25]. The remaining signal after the Butterworth filter effectively consists of frequencies between $0.05 - 35$ Hz, corresponding to the most visible frequency band of flicker [14, 27].

The last filter in Block B is a bandpass filter with a 10 Hz peak. This filter is specifically made to mimic the frequency response of the average observer to a flicker [18]. The three filters of Block B and the resulting bandpass curve of Block B can be seen in Figure 2. The resulting filtration passes mostly frequencies between 5-30 Hz, while severely attenuating outside of this range. The peak of the bandpass is around 10 Hz, which means that the human eye is most sensitive to flicker around this frequency.

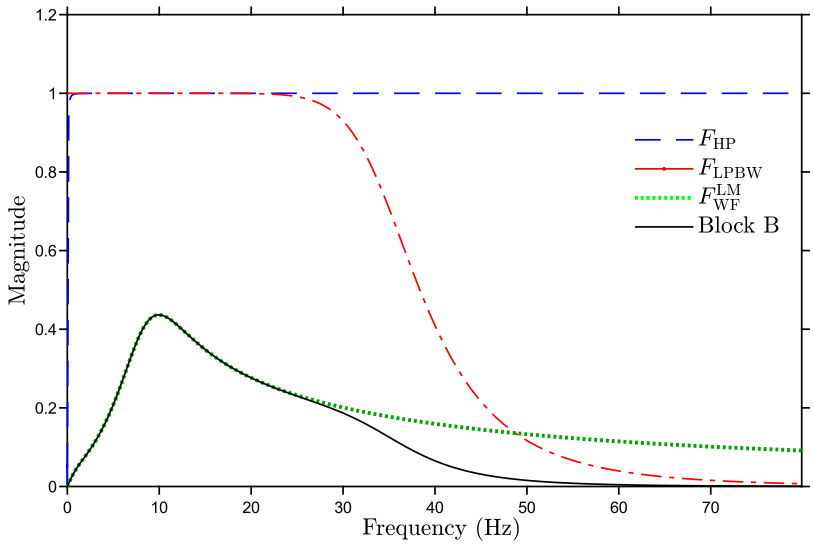

Figure 2. Individual linear-scale amplitudes of filters in Block B, noted as F_{HP} for the high-pass filter, F_{LPBW} for the low-pass Butterworth filter and finally the bandpass filter F_{WF}^{LM}. The combined total amplitude response of the filters in the Block B is shown as the solid black curve (from Publication 1).

The next block, Block C, models the eye-brain response for the signal coming from Block B. Block C used in IEC 61547 [18] is the same as described in Block 4 in IEC 61000-4-15 flickermeter [18, 26]. To consider the nonlinearity of flicker perception when the signal is travelling from the eye to the brain, the signal is squared [25, 26]. This signal is then filtered by a 1st order low-pass filter defined as

$$F_{LP}(s) = \frac{1}{\tau_{LP}s+1}, \tag{2}$$

where $\tau_{LP} = 300$ ms is the time constant for the filter. This filter mimics the brain memory storage effect by merging the fast changes in the flicker severity [25] and creates the unscaled instantaneous flicker sensation [18].

The filtered signal is multiplied with a scaling factor S_0 which is calculated by using an illuminance waveform

$$E(t) = 1 + \frac{d_E}{2}\sin(2\pi f_m t), \tag{3}$$

where $d_E = 0.006832$ is the peak-to-peak amplitude for a sinusoidal wave with $f_m = 8.8$ Hz modulation frequency, so that the maximum instantaneous flicker gets value of

$P_{\text{inst}} = 1$ [25]. However, there is a more practical way to calculate the scaling factor directly from the filter amplitude responses of the flickermeter. Scaling factor is then

$$S_0 = \frac{2}{\left(\frac{d_E}{2} \cdot |F_{HP}(j\omega_m)| \cdot |F_{LPBW}(j\omega_m)| \cdot \left|F_{WF}^{LM}(j\omega_m)\right|\right)^2 \cdot (1 + |F_{LP}(j\omega_m)|)}, \quad (4)$$

where $j = \sqrt{-1}$, $\omega_m = 2\pi f_m$, and $F_{HP}, F_{LPBW}, F_{WF}^{LM}$ and F_{LP} are the filter transfer functions displayed in Figure 2. The resulting instantaneous flicker sensation P_{inst} is the output of Block C.

Block D uses the output of Block C and calculates the P_{st}^{LM} for the input signal. This is achieved by dividing the P_{inst} values into 2^{12} vertical bins and calculating the cumulative distribution function (CDF). The P_{st}^{LM} is calculated as

$$P_{st}^{LM} = \sqrt{0.0314P_{0.1} + 0.0525P_{1S} + 0.0657P_{3S} + 0.28P_{10S} + 0.08P_{50S}}, \quad (5)$$

where parameters P_q describe the values of P_{inst} above which q % of the P_{inst} values are located, i.e. P_5 would describe all P_{inst} values that lie above 5 % of the total P_{inst} values during the measurement period [24]. Smoothing, denoted as suffix S, is used to combat the sudden changes in cumulative probability. The smoothed parameters in Equation (5) are calculated as [18]

$$P_{1S} = \frac{P_{0.7} + P_1 + P_{1.5}}{3}, \quad (6)$$

$$P_{3S} = \frac{P_{2.2} + P_3 + P_4}{3}, \quad (7)$$

$$P_{10S} = \frac{P_6 + P_8 + P_{10} + P_{13} + P_{17}}{5}, \quad (8)$$

$$P_{50S} = \frac{P_{30} + P_{50} + P_{80}}{3}. \quad (9)$$

The first parameter, $P_{0.1}$, is not smoothed as the filter F_{LP} in Block C already has smoothed the sharpest peaks of the signal for $P_{0.1}$.

2.1.1.1 Creating a novel light flickermeter

As described in Publication 1, we found anomalies in the light flickermeter digital implementation [20] recommended in the IEC TR 61547-1:2020 [18]. The main cause of the problems in the flickermeter implementation [25], was caused by how the filters were created in Block B and Block C in MATLAB, which was the programming language used to create this digital implementation. The MATLAB functions *butter()* and *filter()* used to create the filters in the software have limitations depending how they are implemented that

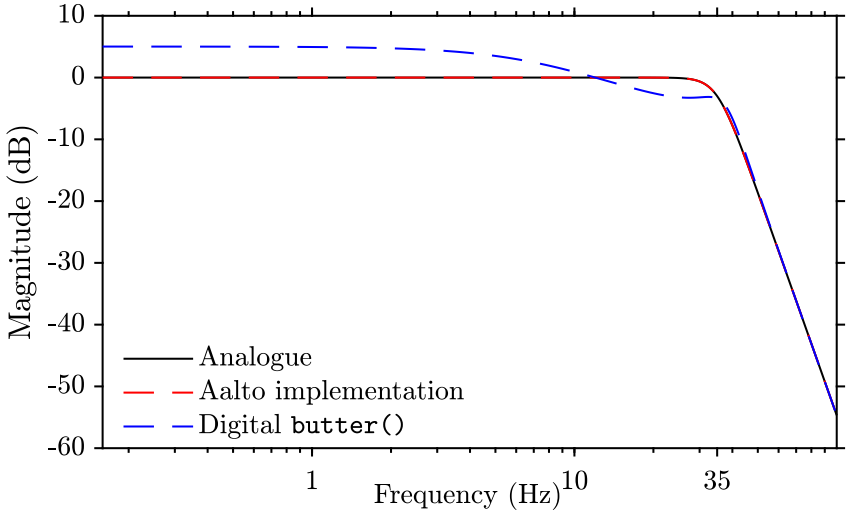

Figure 3. Responses of 6th order low-pass Butterworth filters (from Publication 1).

can cause rounding errors in the filter transfer functions, which causes deviations in the resulting $P_{\mathrm{st}}^{\mathrm{LM}}$. This can be seen especially in the 6th order Butterworth filter, Figure 3, where the blue dashed line is the digitized Butterworth filter made with *butter()* function. This filter response curve does not follow the analogue Butterworth filter curve. To solve this problem with filters and other smaller anomalies within the original software, we created a novel digital implementation, the Aalto flickermeter [17]. We created this digital implementation in MATLAB in accordance with IEC TR 61547 [18].

In Block A, we decided to use MATLAB *mean()* function instead of the low-pass filter in Equation (1) for the normalization of the original signal. This was a practical choice as filtering was deemed to be a possible issue in MATLAB. We decided to subtract the DC component of the signal by subtracting 1 from the normalized signal, i.e. creating a zero-mean signal. This also reduces the transient period in Block B high-pass filter due to removing the need for step-down in the signal from a mean value of one. This technique was implemented also in [20].

For the issue of filtering, Tustin's method was selected to create the filters in the Aalto flickermeter [28]. Using Tustin's method, the analogue filter transfer functions of the filters in Block B and Block C are changed. Firstly, the Laplacian variable s is defined by transformation

$$s = \frac{2}{T_s} \cdot \frac{z-1}{z+1}, \tag{10}$$

where $T_s = 1/f_s$ is the sampling period for a sampling frequency f_s, and z is the complex Z-domain variable [28]. In MATLAB, the transformation is achieved by using the function *bilinear()*. Function *bilinear()* takes zeros, poles and gain of the analogue filter transfer function along with the sampling frequency to create a discretized filter in the zero-pole-gain-representation (ZPK). The practical filtering of the signal is achieved by using *lsim()*-function, which takes the filter transfer function in ZPK format. In the Aalto flickermeter, the sampling frequency is a given variable, thus these filter transfer functions are always calculated to match the real measurements.

We evaluated the transient effects of the Aalto flickermeter. In IEC TR 61547, it is stated that Block A's illuminance adapter would be the main cause of the filter's transient response [18]. Therefore, it is recommended to disregard the first 60 seconds of the P_{inst} data [18]. However, in the case of the Aalto flickermeter, we circumvented the traditional filters in Block A, thus having a possibility to reduce the transient effects. When we plot the illuminance waveform as a function of time from Equation (3) with modulation frequency $f_m = 8.8\,\text{Hz}$ and modulation depth $d_E = 0.006832$ and input it into the Block A, we can find the effect of the transient caused by Block A. As stated in Publication 1, the transient effect was found to settle at approximately 20 seconds with the Aalto flickermeter. Therefore, in the Aalto implementation of the flickermeter, only the first 20 s of P_{inst} is discarded, thus reducing the required measurement time.

2.1.1.2 Validation of the Aalto flickermeter

IEC TR 61547-1 gives five test waveforms with known expected values for testing of flickermeters [18]. For each waveform created by the parameters given in Table 1, the modulation depth is scaled with factors $\alpha = 1/4, 1/2, 1, 2, 3, 4$ and 5. The factor α acts as the target value for the waveform that is fed into the flickermeter, i.e. if we scale modulation depth with α, the expected value of P_{st}^{LM} becomes α.

We ran all 35 waveforms through both flickermeter implementations and calculated absolute deviations for each result. The results can be seen in Table 1. The Aalto implementation outperforms the IEC recommended implementation in all cases, on average having deviations decreasing by an order of magnitude, the IEC recommended implementation having the average deviation of -0.05 while the Aalto implementation has average deviation of +0.003 from target values.

The results show the internal bias in the software implementations, as most of the IEC recommended implementation's deviations are negative, while the Aalto flickermeter deviations are all positive. In IEC recommended implementation, the bias seems to be related to the modulation frequency of the input waveform, as each waveform 1-5 have increasing modulation frequency. The deviations get closer to zero at waveform 3, and

finally with waveform 5, the deviations are positive values for IEC recommended implementation.

Table 1. Deviations from target values for flickermeter implementations. IEC refers to IEC recommended implementation. Waveforms were generated with 200 s length and 50 kHz sampling frequency (from Publication 1).

Waveform	**1**		**2**		**3**		**4**		**5**	
Target value α	IEC	Aalto	IEC	Aalto	IEC	Aalto	IEC	Aalto	IEC	Aalto
¼	-0.0100	0.0007	-0.0105	0.0004	-0.0096	0.0002	-0.0019	0.0003	0.0057	0.0009
½	-0.0197	0.0012	-0.0206	0.0005	-0.0206	0.0001	-0.0024	0.0004	0.0111	0.0015
1	-0.0401	0.0023	-0.0417	0.0009	-0.0411	0.0001	-0.0044	0.0007	0.0201	0.0029
2	-0.0849	0.0045	-0.0815	0.0018	-0.0803	0.0002	-0.0116	0.0014	0.0433	0.0053
3	-0.1375	0.0068	-0.1287	0.0026	-0.1262	0.0002	-0.0212	0.0021	0.0551	0.0072
4	-0.1802	0.0090	-0.1793	0.0035	-0.1660	0.0003	-0.0207	0.0028	0.0729	0.0087
5	-0.1939	0.0113	-0.2062	0.0043	-0.1892	0.0004	-0.0168	0.0035	0.1074	0.0098

As the Aalto flickermeter implementation takes only two parameters, the light waveform, and the sampling frequency, as input parameters, we decided to test the meter as a function of sampling frequency. We created a matching set of waveforms used for the validation of the flickermeter, only changing the sampling frequencies used to create the waveforms from 4 kHz to 100 kHz. For each sampling frequency, we took an average of the normalized deviation from the target values α for both the Aalto implementation and the IEC recommended implementation to compare the performance in this sampling frequency range. The resulting $P_{\mathrm{st}}^{\mathrm{LM}}$ values from the implementations were normalized by dividing the result with α to make it possible to compare deviations across the range. Given the variability in sampling frequencies across different measurement equipment, the flickermeter must have minimal computational error irrespective of the sampling rate used during the measurements.

Results of comparison can be seen in Figure 4. Both implementations are producing deviations around 0.001 on average for sampling frequencies between 4-25 kHz. However, after 30 kHz, the IEC recommended implementation starts to produce deviations over 0.01 from the expected values while the Aalto flickermeter deviations remain an order of magnitude smaller. At around 50 kHz, the deviations for the IEC recommended implementation increase to 0.05 and finally, the software stops working after 70 kHz. The Aalto implementation is stable in this frequency range, having an average deviation of 0.0028 from the target value at 100 kHz sampling frequency.

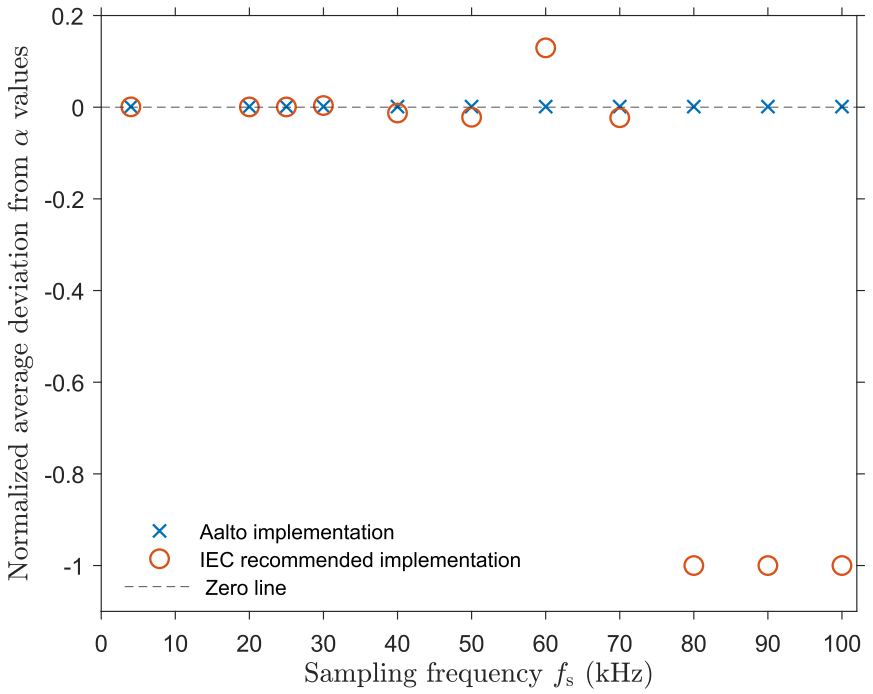

Figure 4. Average deviation from the target value α as a function of sampling frequency. Each deviation is normalized by dividing the value given by the implementations by α (from Publication 1).

2.1.2 Stroboscopic effect visibility meter

Similarly to the flickermeter, IEC TR 63158 [19] describes the M_{vs} meter with four Blocks A-D, as can be seen in Figure 5. Block A is the same input adapter as is used in the flickermeter, normalizing the input signal with the mean value of signal, and outputting the normalized light waveform.

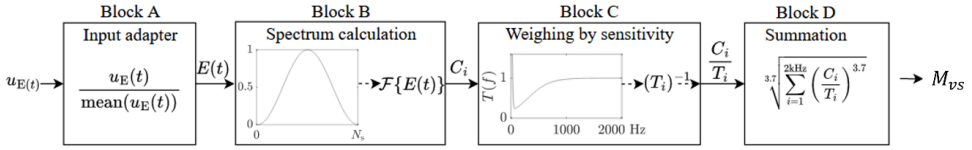

Figure 5. Block diagram for stroboscopic effect visibility meter according to IEC TR 63158 [19] (from Publication 1).

In Block B of the stroboscopic effect visibility meter, the frequency spectrum $C(f)$ is calculated from the normalized light waveform. This is achieved by using discrete Fourier transform (DFT), as the light waveform data is discrete and for AC fed LEDs, it is in practice periodic. Fast Fourier transform (FFT) algorithms have been widely used for DFT to acquire the frequency spectrum, as they are among the most efficient algorithms to calculate Fourier transforms [30].

Before the frequency spectrum can be calculated, IEC and CIE recommend using windowing to consider the spectral leakage effects in the sampled data [10, 19]. The windowing recommended to use in this case is so called Hanning windowing, in some literature also called Hann-windowing. If the signal would not be windowed, the first and last datapoints might be at different phases, creating discontinuity which leads to spectral leakage [24, 31]. The Hanning window combats the spectral leakage by attenuating the amplitudes in the start and at the end of the signal, which reduces the spectral leakage in the transition at the endpoint boundary of the signal [28, 29]. The Hanning window is defined as

$$w_{\text{Hanning}} = \sin^2\left(\frac{\pi n}{N_s}\right), 0 \leq n \leq N_s, \tag{11}$$

where n is the sample index integer and N_s is the number of samples in the signal [28].

Using windowing in time-domain signals leads to attenuation of the signal due to coherent power gain. This needs to be considered after the windowing has been done. For the Hanning window shown in Equation (11), the amplitude is attenuated to half of the original amplitude, thus the amplitude correction factor is 2 [29]. Before the DFT, it is also recommended in [19] to have zero-padding added to increase the frequency resolution. Zero-padding adds zeros to the end of the signal, thus adding more frequency bins to the resulting frequency spectrum after FFT.

After the FFT calculation is completed, the light waveform has been transformed to two-sided frequency spectrum $S(f)$. IEC TR 63158 recommends converting this two-sided spectrum to having only positive frequencies by disregarding the negative side of the spectrum and then multiplying the positive side by a factor of two and normalizing the spectrum with the amplitude of the DC component of the spectrum $S(0)$ [19]. Now for $C(f)$, we get an equation

$$C(f) = 2 \cdot \frac{S(f)}{S(0)},\ f \in \left(0, \frac{f_s}{2}\right]. \tag{12}$$

In practice, dividing by the DC component is redundant in this case, as the light waveform was already normalized in Block A, thus $S(0) = 1$. This output of Block B is the normalized frequency spectrum from Equation (12).

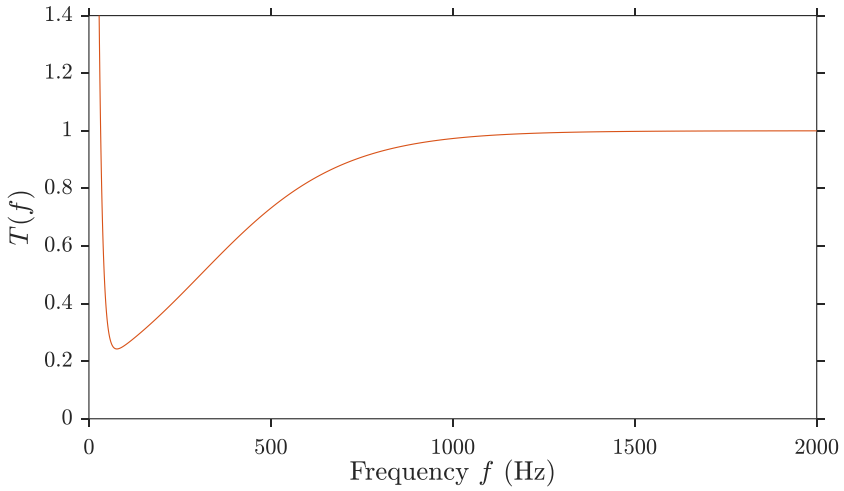

Figure 6. The sensitivity threshold function $T(f)$ for stroboscopic effect.

Block C is used to scale the frequency spectrum with a visibility threshold function. The visibility threshold function is defined as

$$T(f) = \frac{1}{1+e^{-a(f-b)}} + 20e^{-\frac{f}{c}}, \tag{13}$$

where $a = 0.00518$ s, $b = 306.6$ Hz, and $c = 10$ Hz. This threshold is defined between $0 - 2000$ Hz, as can be seen in Figure 6 and thus, the stroboscopic effect visibility measure is not defined beyond 2 kHz. The output of Block C is the weighted spectrum $C(f)/T(f)$.

Block D contains the calculation of stroboscopic effect visibility measure M_{vs} from the weighted spectrum given by Block C. The stroboscopic effect visibility measure is of form

$$M_{\text{vs}} = \sqrt[3.7]{\sum_{i=1}^{N}\left(\frac{C_i}{T_i}\right)^{3.7}}, \tag{14}$$

where C_i is the i^{th} Fourier component of the frequency spectrum and T_i is the component of the sensitivity threshold function evaluated at the frequency of the i^{th} component [19, 30, 31]. The indices i from 1 to N are selected to cover the frequency range of M_{vs} , which extends up to 2000 Hz. The last index N of the summation is selected so that it corresponds to the largest Fourier component with frequency smaller or equal to 2000 Hz [19]. The value of 3.7 in the root and the exponential of Equation (14) comes from the definition of stroboscopic visibility measure in Perz et. al [31], where the visibility of stroboscopic effect was studied.

The Aalto SVM meter [17] was built according to these principles. Originally when Publication 1 was published, the Aalto SVM meter did not have zero-padding implemented, as this was not deemed necessary. However, after user testing, it was brought to our attention that for some on-line measurements, the values dropped unexpectedly with longer acquisition times. Therefore, we added the zero-padding in the software in 2024, which eliminated the issue. This Aalto SVM meter with zero-padding can also be found in GitHub repository [17].

2.1.2.1 Validation of the Aalto stroboscopic effect visibility meter

Similarly to the flickermeter, IEC gives test waveforms for the validation purposes in TR 63158:2018 [19]. However, we used test waveforms given in Dam-Hansen et. al. [22] with more significant digits in the modulation depth and reference M_{VS} (SVM) to reduce rounding errors, thus achieving more accurate assessment of the implementations. There are nine different waveforms, four of which are sinusoidal (Sin) and five square waves (Sqr). Similarly to the validation of flickermeter, we tested both the IEC recommended and the Aalto SVM meter implementations with these waveforms. The test waveform parameters and the results as presented in Publication 1 can be seen in Table 2.

Table 2. Results of the IEC and the Aalto SVM meter implementations with 9 reference waveforms with signal length of 200 seconds and sampling frequency of 50 kHz. The parameters for the test waveforms are: f_m is the modulation frequency and m_{ver} is the amplitude of the waveform. Parameter M_{VS}^{E} is the expected SVM value for the waveform and M_{VS}^{IEC} and M_{VS}^{Aalto} are the SVM values of these implementations. Digits highlighted with red show the difference between the number of significant digits between IEC 63158:2018 [19] and Dam-Hansen et.al. [22] in the reference waveform values.

Waveform	f_m (Hz)	m_{ver}	M_{VS}^{E}	M_{VS}^{IEC}	Deviation	M_{VS}^{Aalto}	Deviation
Sqr-1	99	0.20049200	1.000000	0.9782	-0.0218	1.0000	0.0000
Sqr-2	100	0.20119076	1.000000	0.9983	-0.0017	1.0000	0.0000
Sqr-3	100	0.0201119076	0.100000	0.0998	-0.0002	0.1000	0.0000
Sqr-4	100	0.80476304	4.000000	3.9922	-0.0078	3.9996	-0.0004
Sqr-5	101	0.20189857	1.000000	0.9945	-0.0055	1.0000	0.0000
Sin-1	32	1	0.990565	0.9929	+0.0023	0.9905	-0.0001
Sin-2	100	0.25627533	1.000000	0.9982	-0.0018	1.0000	0.0000
Sin-3	500	0.73141469	1.000000	0.9925	-0.0075	0.9998	-0.0002
Sin-4	1900	0.99973980	1.000000	0.9935	-0.0065	0.9963	-0.0037

The Aalto SVM meter has significantly smaller deviations from the expected values than M_{VS}^{IEC}. On average for the Aalto implementation without zero padding implemented, the absolute deviations decreased for the sinusoidal waveforms from 0.0045 to 0.0010 and for square waves, from 0.0074 to 0.0001.

Now, if we compare the results to the newest version of Aalto SVM meter with zero-padding, represented in Table 3, we can see that zero-padding reduces the deviation in the Sin-4 waveform, which had the worst deviation in the original Aalto SVM meter, while decreasing also Sqr-4 waveforms deviation, and only increasing the deviation of Sin-3 by 0.0001. This implementation with zero-padding has been added to the GitHub database [17]. Now the average deviation of Aalto SVM meter is 0.00001 for square waves, and for sinusoidal test waveforms it is -0.0001.

Table 3. Deviations of the Aalto SVM meter without zero-padding and with zero-padding (notated as $M_{VS}^{Aaltozp}$) of 15 times the original signal length. The signals were created with 200 second signal length and 50 kHz sampling frequency.

Waveform	M_{VS}^{E}	M_{VS}^{Aalto}	Deviation	$M_{VS}^{Aaltozp}$	Deviation
Sqr-1	1.0000	1.0000	0.0000	1.0000	0.0000
Sqr-2	1.0000	1.0000	0.0000	1.0000	0.0000
Sqr-3	0.1000	0.1000	0.0000	0.1000	0.0000
Sqr-4	4.0000	3.9996	-0.0004	4.0000	0.0000
Sqr-5	1.0000	1.0000	0.0000	1.0000	0.0000
Sin-1	0.9906	0.9905	-0.0001	0.9906	0.0000
Sin-2	1.0000	1.0000	0.0000	1.0000	0.0000
Sin-3	1.0000	0.9998	-0.0002	0.9997	-0.0003
Sin-4	1.0000	0.9963	-0.0037	0.9999	-0.0001

2.2 Measuring Temporal Light Artefacts

The TLA measurements are based on photometry, i.e. the measurements of light detectable by human vision. The SI base unit for photometry is the candela (cd), the unit of luminous intensity I_v. The Bureau International des Poids et Mesures (BIPM) has given the definition of candela as "… the SI unit of luminous intensity in a given direction. It is defined by taking the fixed numerical value of the luminous efficacy of monochromatic radiation of frequency 540×10^{12} Hz, K_{cd} to be 683 when expressed in the unit lm W^{-1}, which is equal to cd sr W^{-1}, …" [32]

The frequency of 540×10^{12} Hz mentioned in the definition corresponds to the wavelength of light at 555 nm in air, which is the approximate peak of the photopic responsivity curve $V(\lambda)$, defined by CIE [33] and sr (steradian) is the solid angle unit. There are multiple

quantities in photometry that are related to the base unit candela. First there is luminous flux Φ_v with the unit of lumen (lm), which describes the total amount of emitted light from a light source in all directions. From luminous flux, we can derive illuminance E_v with a unit of lux (lx or lm m^{-2}). Illuminance is the luminous flux i.e. the amount of light that hits a defined surface area.

2.2.1 Measurements of temporally modulated light according to standards

IEC and CIE recommend using illuminance or luminous flux to measure TLA parameters [13, 18, 19]. In the measurement of TLAs, we are mostly interested in the relative temporal light waveform. Therefore, the photometric quantity in the end does not matter apart from the implementation and equipment standpoint. Measuring the relative light waveform also means that there is no need for absolute photometric characterization of the measurement setup.

We realized TLA measurements using the setup shown in Figure 7. We opted to use the luminous-flux-based measurement setup, as the IEC TR 63158:2018 [19] recommends indirect measurement of light, to consider the possible non-uniform distribution of light coming out of the source itself. The integrating sphere used for the measurements provides natural optical shielding, which reduces the stray light in the measurements, and due to its aluminium shell, it provides also shielding from electromagnetic interference mentioned in [19]. The lamp, referred to as device under test (DUT) in Figure 7, is set into the centre of the integrating sphere, and is driven by a Chroma 61601 programmable AC power source [34]. The attached power analyser was used to acquire the current waveform data from the measured DUT and to monitor the input current and voltage from the AC power source.

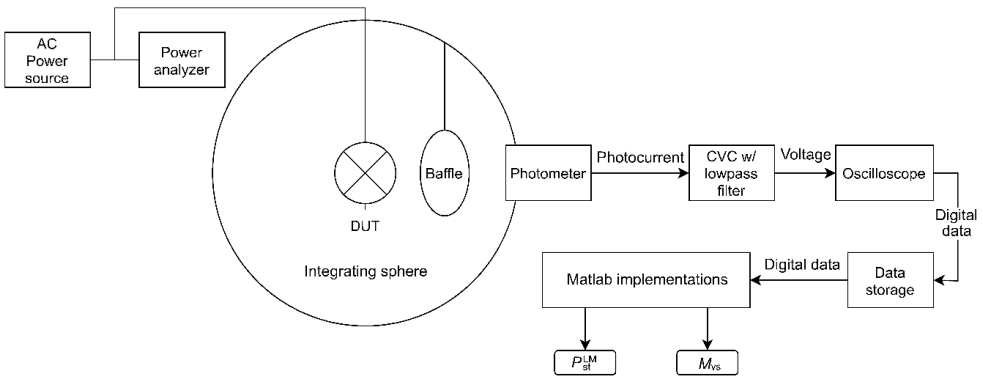

Figure 7. Schematic of the realized TLA measurement setup (from Publication 3).

For detection, we used a photometer, PRC TH15 manufactured by PRC Krochmann GmbH, Germany. This photometer consists of an 8-mm diameter flat diffuser as light collecting surface, a temperature controlled $V(\lambda)$-filter, and a silicon photodiode. The resulting photocurrent on the photodiode consists of the light that the diffuser surface gathers, gets transmitted through the filter and hits the photodiode surface. The amount of photocurrent created is small, usually having an order of magnitude of 10^{-9} amperes per lux, i.e. for each unit of illuminance hitting the photodiode, we get few nanoamperes of measurable photocurrent out from the contacts of the photodiode.

We used in-house build current-to-voltage converter (CVC) as an amplifier. The amplifier used has two-phase amplification possibility. First there is a transimpedance amplifier, which converts the current to voltage with selectable amplification between 10^3 to 10^9 V/A. Then there is a possibility to post gain amplification of -1, 10 or 100, which increases the maximum amplification to 10^{11} V/A. This CVC has a built-in low-pass filter that can be used to cut the unwanted high-frequency components from the photocurrent, which is useful for TLA measurements to combat anti-aliasing in the measurements [13,19]. In the CVC the cutoff frequencies f_c for low-pass filter are: 10, 100, 1000 and 10 000 Hz.

For collecting the data, both CIE and IEC [13,19] recommend using an oscilloscope with sufficient resolution for data acquisition. The oscilloscope converts the analogue signal from the CVC to digitized form, working in practice as an analogue-to-digital converter (ADC). The oscilloscope we used has an internal storage to store measured light waveforms that can be later downloaded from the device for TLA calculations. The oscilloscope is also used to define the sampling frequency f_s from the acquisition time T_m, and number of samples N_s by equation

$$f_s = \frac{N_s}{T_m}. \tag{15}$$

By selecting suitable values for T_m, N_s and f_c, we can reduce the effects of anti-aliasing. For our measurements, we selected $T_m = 200$ s, $N_s = 10^7$ and $f_c = 10$ kHz [35], giving the resulting sampling frequency $f_s = 50$ kHz. These settings were used in Publication 3 for the measurements of commercial lamps.

2.2.2 Camera-based measurement methods

Sometimes the light source cannot fit into the integrating sphere, or there might be other sources close by, which would make measurements in the traditional way difficult, if not impossible. Recently there have been novel methods proposed to measure a single light

source using a phase locked spectrometer that can detect low level signal from a complex measurement scenario such as outdoor lights during daytime [36]. However, by using a camera-based system, measurement of multiple sources could be achieved, which has recently been shown in a study [37] where TLAs were measured with a high-speed camera from multiple sources using an equivalent time sampling (ETS) with two different triggering methods, continuous-trigger method and delay-trigger method.

On the other hand, spectrally resolved measurements of TLA sources could be beneficial in future, as many LED sources with tuneable colour are made with multiple different colour LED sources inside the housing of the lamp. These can be either red, green, blue (RGB) LEDs or more recently red, green, blue and white (RGBW) LEDs. In the case of these kinds of sources, it could be useful to know the main contributor for the TLA behaviour with a single measurement of the sources. This could be achieved by utilizing a hyperspectral camera, which has the benefit of measuring wide range of spectrum, while having the potential to measure multiple sources simultaneously. By using a triggering implementation similarly to [37], we could produce TLA measurements within narrow spectral bands to see the potential differences in TLA behaviour across the spectrum by utilizing a hyperspectral camera.

The main downside of hyperspectral camera for these kinds of measurements is that the cameras are relatively slow. For example, Senop HSC-2 hyperspectral camera [38], has a maximum framerate of 149 frames per second (fps), which is not enough to fulfil the Nyquist criterion [28] for measuring phenomenon with maximum frequencies of 2 kHz [10]. Therefore, we need to increase the sampling frequency when using the hyperspectral camera to measure TLA effects. Although stroboscopic effect takes all frequencies up to 2000 Hz into consideration, often high frequency components are not present in the source. For example, in Figure 8, we can see that the source DUT1 measured in this work has frequency components only up until 300 Hz, which means that to fulfil Nyquist criterion, we only need sampling rate of 600 Hz. The dominant frequency of DUT1 is 100 Hz.

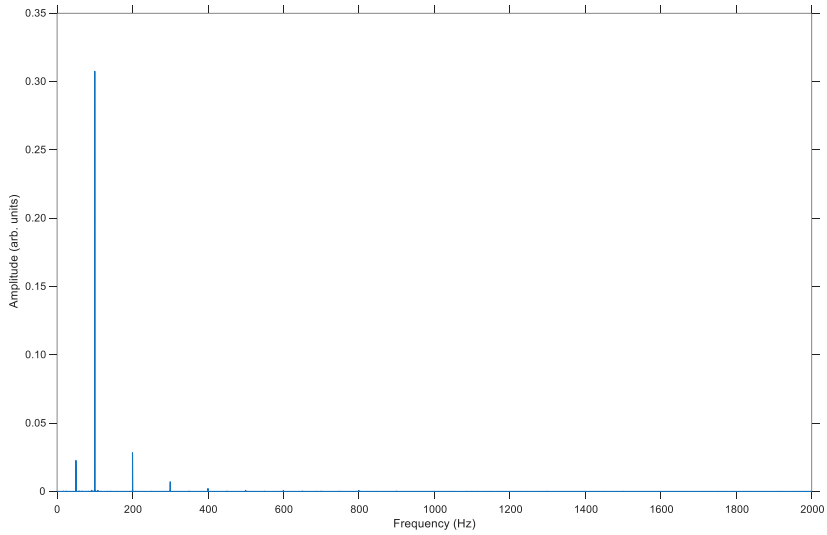

Figure 8. Fourier transform of the measured light waveform of DUT1. DUT1 has dominant frequency of 100 Hz (From publication 2)

Senop HSC-2 hyperspectral camera has one-megapixel resolution (1024 pixels x 1024 pixels) with 12-bit dynamic range. When using the "narrow" bandpass setting of the camera, one can achieve around 10 nm full-width half maximum (FWHM) for the three spectral lines used to measure the TLA in this study; 450, 550 and 650 nm. It also has an external trigger function, which allows us to use other devices to give a signal for the camera to initiate measurements, like the delay-trigger method given in [37]. If we take a measurement sequence with a speed of 100 fps, starting from any selected point on the signal, and then introduce next measurement sequence from the same phase of the signal but adding a small delay before sending the trigger signal, we can scan more of the signal than we could with just 100 fps. By adding these delayed signals, we can increase the sampling rate, thus collecting more of the signal.

Forming and collection of delayed signals is demonstrated in Figure 9. If we trigger the first measurement at the green square, our measurement will measure the signal at the measurement interval of the device, i.e. the other green squares. If we then trigger the measurement again, but add a delay d, we measure all the red squares of the signal, and so forth. By combining the gathered waveforms, we get the original signal with effectively higher sampling rate, thus enhancing the Nyquist criterion to higher frequencies.

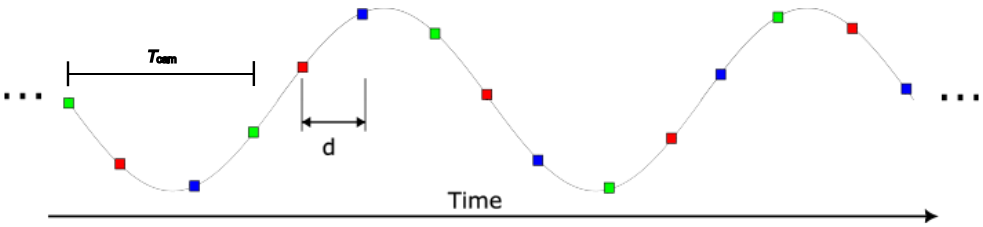

Figure 9. A visual example of sampling of a sinusoidal waveform with delay-trigger method. The different colours of squares describe the different measurement sequences, *d* is the delay between two measurement sequences, and $T_{\mathrm{cam}} = \frac{1}{f_{\mathrm{cam}}}$ is the period between frames from the camera. (From publication 2)

We used one of the studied lamps as the reference for triggering. A photometer was monitoring the lamp from outside of the field of view (FOV) of the hyperspectral camera, positioned so that it only detects light from the reference lamp. The photocurrent was sent to an Arduino Uno microcontroller as a reference signal, from which we controlled the triggering using a software to do measurements automatically. When the software detects a pre-defined value on the rising signal around the "zero-crossing" of the sinusoid, it sends a trigger signal to the hyperspectral camera and waits for the measurement to finish. The software waits for the same trigger point as in the previous round, but this time adds a small delay to the trigger signal of the camera. The sequence is repeated until the desired number of measurements is achieved.

The resulting effective sampling frequency is given by the Equation (15), however, T_{m} is not directly the measurement time of a sequence, but is defined by the equation

$$T_{\mathrm{m}} = N_f T_{\mathrm{cam}} + (k-1)d \tag{16}$$

where k is the number of measurement iterations, d is the delay between measurements, N_f is the number of frames measured. In practice, this adds $(k-1) \cdot d$ seconds to the original measurement length. Now if we rewrite Equation (15), we get

$$f_{\mathrm{s}} = \frac{kN_f}{T_{\mathrm{m}}} = \frac{kN_f}{N_f T_{\mathrm{cam}} + (k-1)d}. \tag{17}$$

In this work we used $k = 10$, $d = 1$ ms, $N_f = 100$ frames and $T_{\mathrm{cam}} = 10$ ms. Now we can get the effective sampling frequency 991 Hz from Equation (17).

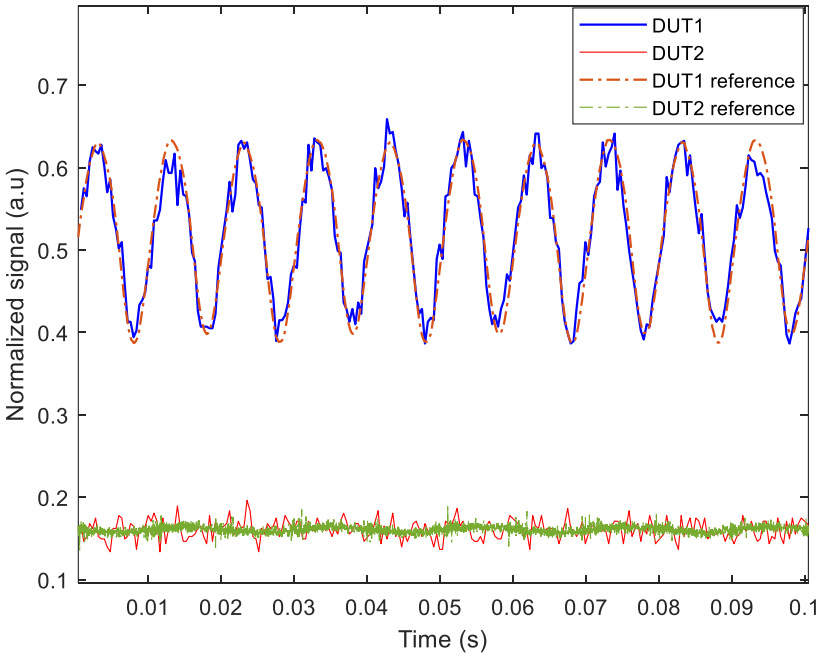

Figure 10. Measured signals with the hyperspectral camera at 450 nm and the reference waveform from the integrating sphere setup for light sources DUT1 and DUT2. Reference waveforms were measured with 1 kHz sampling frequency and with measurement time of 200 seconds. (from Publication 2).

However, one should take care when selecting the delay interval for the measurement, as one might find that the delay starts overlapping with the previously measured sections of the waveform. As the first point of 10^{th} delay increment already overlaps with the second frame of the first measurement when delay is set to 1 ms, this reduces the effective sampling frequency. To increase the sampling frequency in the measurement, one should select the delay parameter so that it does not overlap with previous measurement points of the signal, at least until the desired sampling frequency has been achieved. For example, decreasing the delay interval from 1 ms to 0.25 ms would increase the effective sampling frequency to roughly 4000 Hz, which should decrease the effect of aliasing in the measured signal.

From the resulting hyperspectral images, we reconstructed the signal with MATLAB software, developed to arrange the images into the correct temporal order, which allows calculating the light waveform for each pixel. However, due to the large data sets in hyperspectral imaging, this is done to a single selected pixel in the image to reduce the running time of the script. The reconstructed signals for DUT1 and DUT 2 can be seen in Figure 10 with reference waveforms measured with the setup described in 2.2.1. As can be

seen from Figure 9, the dominant frequency component of DUT1 is seen clearly as the sinusoidal has a period of roughly 100 Hz.

From the collected signals from DUT1 and another source DUT2, seen in Figure 10, we can calculate the TLA parameters using the Aalto implementations of TLA meters described in Publication 1. These lamps had colour temperature of 2700 K. We also measured the reference values using the integrating sphere setup described in Chapter 2.2.1 and calculated the TLA parameters used as reference values for both DUT lamps. Then we compared the results of the hyperspectral camera to these reference values, the results of which can be seen in Table 4.

The average $P_{\mathrm{st}}^{\mathrm{LM}}$ and M_{vs} values for DUT1 are within 3 % of the reference values, which is relatively close. However, for the DUT2, the $P_{\mathrm{st}}^{\mathrm{LM}}$ value deviates more, around 5 %, and M_{vs} has 54 % deviation from the reference value. This deviation could be due to the shape of the waveform of DUT2 seen in Figure 10, showing the small amplitude of the signal, thus reducing the modulation depth. The frequency spectrum of DUT 2 has the main peak at 50 Hz, i.e. the mains frequency, but it has a lot of smaller peaks across the frequency band of interest that affect the shape and complexity of the waveform (Publication 2). As the hyperspectral camera measurements have sampling frequency of 991 Hz, the peaks of the signal that are higher than 495 Hz are not properly taken into account in the measurement of M_{vs}, which likely causes the differences in DUT2 M_{vs} value. As M_{vs} considers higher frequencies compared to $P_{\mathrm{st}}^{\mathrm{LM}}$, this loss in the high-frequency components affects M_{vs} more than $P_{\mathrm{st}}^{\mathrm{LM}}$. One possible solution could be to take triggering directly from the line voltage driving the sources, to which the TLAs may be synchronized. As the original purpose of the research for Publication 2 was to create a measurement system to measure fixed lighting fixtures, such as ceiling lights in the office, this was not utilized in the Publication 2.

It should be noted that according to IEC technical report, the measurement time used in the hyperspectral camera measurements are not within recommendations for $P_{\mathrm{st}}^{\mathrm{LM}}$. The recommended measurement time is at minimum > 60 seconds to combat transient period of the filters in the flickermeter. However, with the hyperspectral camera, we are limited with the data storage. A single wavelength measurement with the measurement parameters used takes 10 GB of storage. If we would assume that all measurement frames take same storage space, we would need 600 GB of storage for a minute of measurements. This would limit the measurements to a single waveform at a time due to the camera's internal storage limit of 1 TB. As can be seen from Table 4, the measurements seem to work sufficiently for the sources measured in this work.

Table 4. Values of $P_{\mathrm{st}}^{\mathrm{LM}}$ and M_{vs} measured with the hyperspectral camera for the test lamps at three wavelengths and the average values of these for the two measured lamps, and the reference TLA values measured with the integrating sphere setup. (from Publication 2)

Wavelength [nm]	DUT1 $P_{\mathrm{st}}^{\mathrm{LM}}$	DUT1 M_{vs}	DUT2 $P_{\mathrm{st}}^{\mathrm{LM}}$	DUT2 M_{vs}
450	0.542	0.680	0.128	0.169
550	0.308	0.415	0.077	0.174
650	0.435	0.453	0.084	0.083
Average	0.428	0.516	0.097	0.142
Reference	0.418	0.532	0.102	0.307

3 Effects of regulation on commercial light sources

The Ecodesign regulation set the limits for P_{st}^{LM} and M_{vs} for consumer grade LED lamps, which are mains connected and operated at full power, starting from September 2021. For flicker, the limit was set to $P_{st}^{LM} < 1$, which means that the flicker is, on average, not visible from the light source. For M_{vs} the limits were set in two phases, first from September 2021 to September 2024 the limit was $M_{vs} < 0.9$ and in September 2024, it was reduced further to $M_{vs} < 0.4$ [5]. In this chapter, we discuss the effects of this regulation on P_{st}^{LM} and M_{vs} values before and after the regulation was set, by comparing TLA measurements of LED lamps that were purchased on the EU market before and after the regulation.

We studied various LED lamps produced both before and after September 2021. The lamps were divided into four groups according to their driver topologies which will be discussed in Chapter 3.1. This was done to see the practical solutions that manufacturers have made to potentially improve the TLA characteristics of their light sources and comply to the regulations. The measurements and a comparison of the TLA characteristics of pre- and post-regulation lamps are described in Chapter 3.2. These are findings that were published in Publication 3.

3.1 Driver topologies for classification of commercial LEDs

LEDs are driven on DC, which requires AC-to-DC conversion in the drivers of the LED sources. The LED lamps can be divided into four main groups by their driver types as described by Xu et. al. [39], and as shown in Figure 12. The stability of the driver output current has direct impact on the luminous output of the LED source, thus impacting the TLA behaviour of the LED [9]. In Figure 12, the circuitry shows only one LED string. However, it is very common to have multiple LED strips or filaments attached to the electrical circuitry [39].

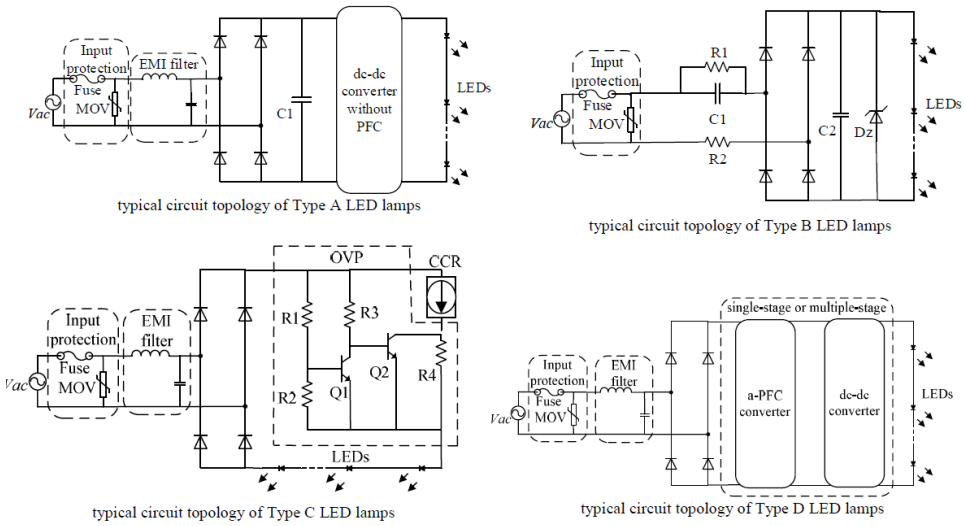

Figure 11. Four basic driver topologies A-D as presented by Xu et.al. [39].

Type A topology is defined as “Full-wave Rectifier with Smoothing Capacitor and DC-DC Converter Circuit” [39]. First there is an input protection circuitry created with a fuse and a metal-oxide varistor (MOV in Figure 11), which is in all topologies A-D. After the input protection, there is an electromagnetic interference (EMI) filter, achieved by an L-C circuit, where the combination of an inductor and capacitor create a low-pass filter for the electric current, attenuating the high-frequency components of the AC and reducing EMI. This EMI filter is found also in Type C and D circuit topologies. The AC-DC conversion is achieved with full-wave bridge rectifier using diodes. A smoothing capacitor (C1 in Figure 11) is used to smooth the rectified sinusoid to achieve a smoother DC voltage through the system, acting as an energy storage for the zero-crossings in the AC voltage. Type A topology uses DC-DC conversion to adjust the DC voltage for the LED strip. The shape of the measured input current in Figure 12 is explained by not having power factor correction (PFC) in the driver, which causes the lamp to draw short, but high-amplitude current pulses every half-phase of the input voltage to charge the smoothing capacitor. [39, 40]

The Type B topology is defined as “Capacitive Dropper Circuit” by [39]. Following the input protection, there is a capacitor C1 in series, followed by a full-wave rectifier. Capacitor C1 limits the current and voltage going to the rectifier circuit. There is a resistor R1 parallel to capacitor C1, that discharges the capacitor when electricity is cut off from the mains. The in-series resistor R2 acts as a limiter for the inrush current. Between the rectifier and the LED strip, there is a Zener diode (DZ), which acts as a shunt regulator and protects the LED strip from overvoltage. [39, 40]

Type C is “Linear Constant Current Regulator (CCR) Straight circuit”. This topology is the same as Type A up to the full-wave rectifier circuit, but instead of using a smoothing capacitor, it uses a CCR circuit, which can operate with a wider range of un-smoothed voltages. In Figure 11, electronics within the dashed line are over-voltage protectors (OVP) for the CCR circuit, as it is prone to damage from overvoltage in its transistor configuration. [39, 40]

Type D topology is “Switch-Mode Driver Circuit”, which has the same input protection and EMI filter followed by a full-wave rectifier as Types A and C have. Type D topology drivers have a DC-DC converter with PFC which sets the voltage level for the LEDs. They can further be divided into two subgroups depending on if the DC-DC converter has one or two phases. [39, 40]

The classification by Xu et. al. is not the only available classification. For example, in [9] and [40], there are discussion about different topologies of LED drivers. However, the classification of Xu et. al. [39] was chosen for this work, because it gives the ability to distinguish the different topologies using the input current and input voltage waveforms of the light sources, as can be seen in Figure 12. When the 60 pre-regulation lamps were divided into the groups, 42 lamps were Type A, four were Type B and 14 were Type D. In the new lamps, 18 were Type A lamps, and only 2 lamps were of Type C.

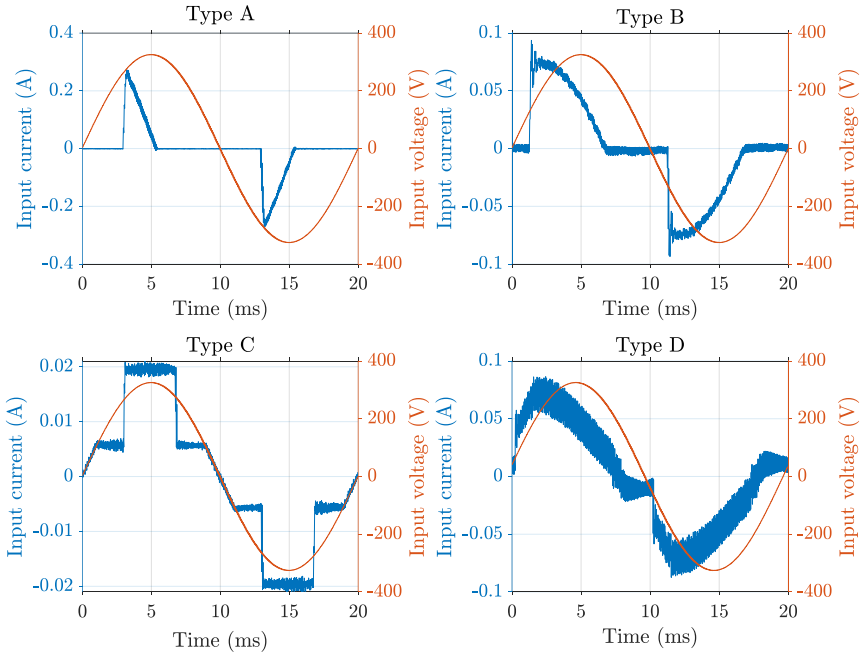

Figure 12. Typical input current and input voltage waveforms for the driver topologies A-D. These waveforms are from measurements of the lamps performed in Publication 3 (from Publication 3).

3.2 Effects of regulations in manufacturing

We measured 80 different LED lamp types, 60 of them manufactured around the year 2016, well before the EU Ecodesign regulation was introduced. Remaining 20 lamp types were purchased in December 2021. All lamps were purchased from different stores in Finland. The lamps were classified to the four topologies according to the current waveforms shown in Figure 12, using the power analyser in the measurement setup described in Chapter 2.2.1. The older set of lamps were produced by 22 different manufacturers, while the 2021 set of lamps had 9 different manufacturers.

We used the interquartile range (IQR) presentation to display the differences in the measured $P_{\mathrm{st}}^{\mathrm{LM}}$ and M_{vs} values between the lamps before and after the Ecodesign regulation. The results are shown in Figures 14 and 15 for $P_{\mathrm{st}}^{\mathrm{LM}}$ and M_{vs} respectively. In these figures, the red line inside the blue box represents the median value of the $P_{\mathrm{st}}^{\mathrm{LM}}$ or M_{vs}, the blue box represents the upper and lower limits of the IQR. As an example, if we have a set of values with a Gaussian distribution, the 25$^{\mathrm{th}}$ and 75$^{\mathrm{th}}$ percentile of the data would be the lower and upper limits of the box presented in Figures 13 and 14, marked as Q_1 and Q_3, while the median Q_2 of the dataset would be presented as the red line inside the box. The IQR is the difference between the upper and lower limits, $\mathrm{IQR} = Q_3 - Q_1$, describing the data in between the 75$^{\mathrm{th}}$ and 25$^{\mathrm{th}}$ percentiles, i.e. the middle 50 % of the data. Now the whiskers describe values below Q_1 and above Q_3, that are within 1.5 x IQR. For lower whisker $\mathrm{IQR}_{\mathrm{w_l}}$, the equation would be written as

$$\mathrm{IQR}_{\mathrm{w_l}} = Q_1 - 1.5 \times \mathrm{IQR}, \tag{18}$$

and similarly for upper whisker,

$$\mathrm{IQR}_{\mathrm{w_u}} = Q_2 + 1.5 \times \mathrm{IQR}. \tag{19}$$

If there is no data point at the exact value, the whisker for $\mathrm{IQR}_{\mathrm{w_l}}$ is set to the lowest datapoint that is greater than $\mathrm{IQR}_{\mathrm{w_l}}$ and for $\mathrm{IQR}_{\mathrm{w_u}}$ the selected point would be set to the highest data point smaller than $\mathrm{IQR}_{\mathrm{w_u}}$. As IQR represents middle 50 % of the values, the whiskers represent the 24.65 % of the values outside IQR for a dataset with Gaussian distribution. Values that are outside of the whisker range are defined as outliers in IQR representation. In Figures 14 and 15, the outliers are shown as red + signs. [42, 43, 44]

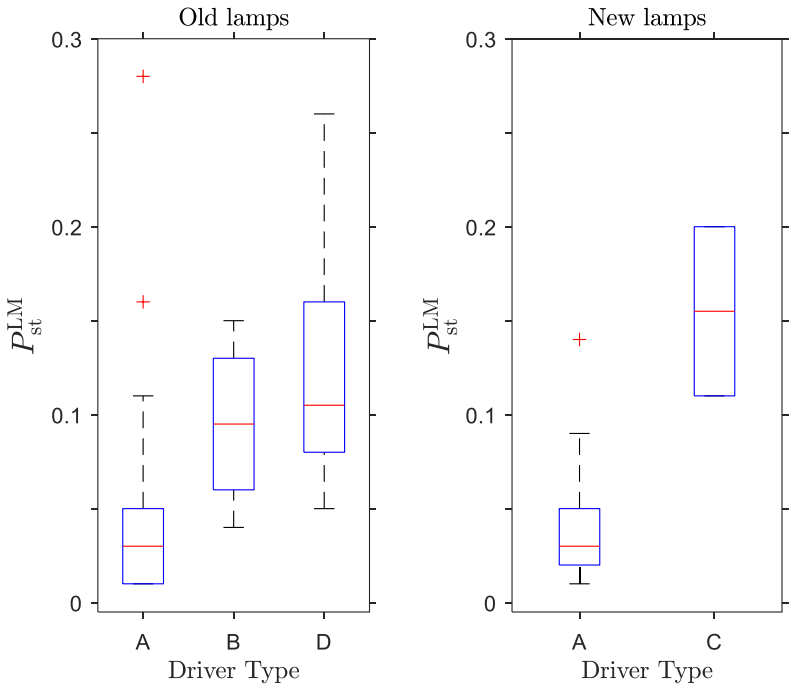

Figure 13. Values of P_{st}^{LM} and driver topologies before and after the Ecodesign regulation was set (from Publication 3).

All P_{st}^{LM} values shown in Figure 13 are well below the EU Ecodesign limit of $P_{st}^{LM} < 1$ with both old and new lamps. Small improvements were made in the Type A lamps, as the median value is slightly lower, the whiskers are a bit shorter, and there are less outliers in newer lamps. Every other type has higher P_{st}^{LM} than the Type A lamps. In the case of older Type A lamps and Type C lamps, the whiskers are not visible, as there are no datapoints after the blue box, thus the IQR_{wl} and the Q_1 are at the same datapoint.

The stroboscopic effect visibility has changed more when comparing the pre-regulation lamps to the post-regulation lamps as can be seen in Figure 14. Here it can also be seen why Types B and D are not seen in the new set of lamps, as they display significantly higher M_{vs} values than A or C types. Type D is on the average the worst, having the median M_{vs} value over 1, whereas Type B has the median value just slightly under the first limit of the EU Ecodesign regulation. Type C lamps, while having worse P_{st}^{LM} values than Types B and D, have significantly better M_{vs} values. However, they might not conform with the limits of the regulation after September 2024. Type A lamps have the best characteristics also in M_{vs}, both in the old and the new set of lamps, having the same trend as in P_{st}^{LM} values, where the difference between old and new lamps is reduction of outliers. Type A lamps, apart from

some outliers in the old lamps have M_{vs} smaller than the regulation limit set in September 2024.

The European Union has requested that the manufacturers that sell consumer lamps inside EU declare the TLA values for their products, which are stored in EPREL database [45]. However, it was found out that in the EPREL database, the values given for P_{st}^{LM} and M_{vs} by the manufacturers are in many cases the same as the Ecodesign limits, i.e. they have given $P_{st}^{LM} = 1$ and $M_{vs} = 0.4$ as the entries, instead of measured values. This could be improved significantly by requesting the manufacturers to give also realistic TLA values in the EPREL database by future regulatory action. There is a significant practical difference between lamps that are close to the TLA limits and lamps that are close to the average Type A light source. This change would make the EPREL database more useful for consumers, as now it tracks just the compliance.

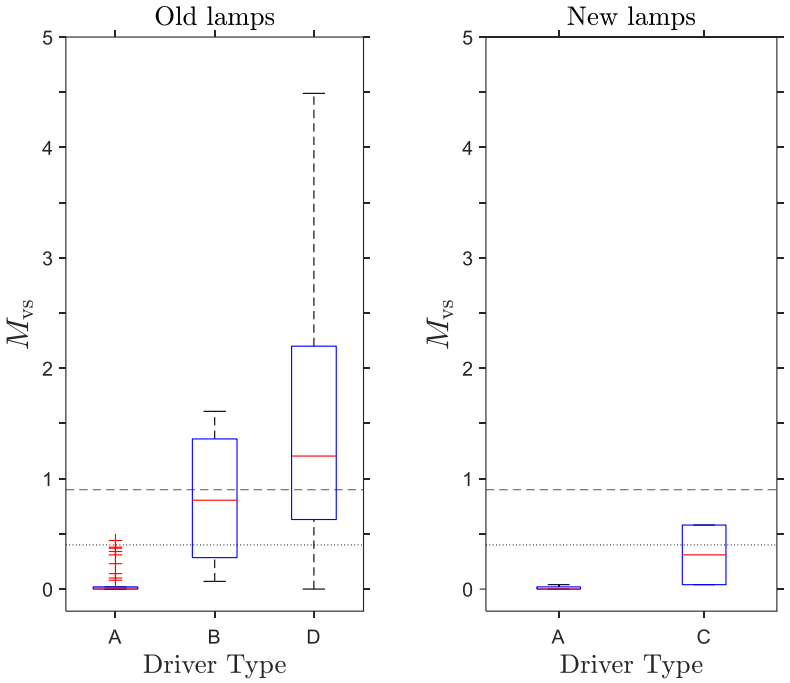

Figure 14. The effect of Ecodesign regulation on M_{vs} values and driver topologies. The dashed line shows the limit from 2021 to 2024. The dotted line shows the limit after September 2024. New lamps with Type A drivers have $0 < M_{vs} < 0.04$ and demonstrate significant improvement in lamp performance (from Publication 3).

4. Conclusions

This thesis presents advancements in the measurement of temporally modulated light sources, covering a broad scope from software development and novel methodologies to practical measurements and the analysis of the regulatory impacts within the European Union. The research provides both practical tools for spectral TLA measurements and refined solutions for the accurate assessment of TLA metrics.

In Chapter 2, the measurements of temporal light artefacts are described. First, in Chapter 2.1, the Aalto TLA meters of Publication 1 are described to enhance the accuracy of existing flickermeter software in alignment with IEC standards. Initial investigations revealed anomalies in the results produced by earlier implementations using the *butter()* and *filter()* functions in MATLAB implementation. To address these issues, new TLA meters were built from the ground up, employing alternative functions *bilinear()* and *lsim()* to improve signal filtering and overall model accuracy. The Aalto TLA meters significantly reduced deviations in the test waveforms prescribed by the IEC. Specifically, the Aalto flickermeter decreased average deviations from -0.05 to +0.003, an improvement of an order of magnitude as compared to the IEC recommended implementation. For the SVM metric, deviations similarly dropped from 0.0045 to 0.0001 for sinusoidal test waveforms, and for square waves from 0.0074 to 0.0000, effectively eliminating deviations in most cases. The Aalto implementations have been made publicly available for anyone to use in GitHub [17].

Chapter 2.2 describes the practical side of the measurements of TLAs. First the conventional integrating sphere-based measurements in Chapter 2.2.1 are described. This measurement method was used in Publication 3 to measure the 80 different lamps to research the effect of the Ecodesign regulation on the lamps before and after the regulation. Chapter 2.2.2 describes how a hyperspectral measurement setup of TLA is implemented as shown in the Publication 2. The hyperspectral camera provides both spatial and spectral measurements that can be useful for more complex lighting scenes, where the types of light sources are unknown. The measurements are less accurate than traditional measurements of TLA, however some lighting fixtures, for example office room lighting, are difficult to measure with traditional measurement setups. Thus, this kind of a setup could produce good enough results for assessing the TLA characteristics, while providing the possibility of TLA measurements at different spectral bands. This work has proceeded on the basis of the previously utilized triggering method with cameras by adding a possibility to measure

distinct spectral bands from the source, which could help to find cause of TLA in multi-colour LED based light sources in the future.

Chapter 3 describes the investigation of impact of the EU Ecodesign regulation had on TLA parameters, $P_{\mathrm{st}}^{\mathrm{LM}}$ and M_{vs}, in consumer lighting. The TLA parameters were reported in Publication 3 for a total of 80 lamp types, 60 acquired before and 20 after the regulation took effect. These lamps were classified into four circuit topology groups (Types A–D), revealing trends in manufacturer adaptation. The findings show a clear shift towards Type A lamps, which dominated both the pre- and post-regulation samples. Types B and D are being phased out, as they had high M_{vs} values beyond the limit set by Ecodesign regulation, while new Type C lamps, characterized by lower M_{vs} values than Types B and D, are emerging, albeit in small numbers (2 of the 20 new lamps).

In summary, this work contributes novel tools, enhances existing measurement systems, and deepens understanding in the field of optical metrology, particularly for temporally modulated light. The methods developed allow for precise evaluation of TLA characteristics across a variety of light sources. Furthermore, the results demonstrate that the EU Ecodesign regulation has led to the improved temporal light modulation characteristics in commercially available lighting, thereby supporting efforts to reduce the adverse health impacts of such light sources on humans.

References

[1] Electric lamp, by Thomas A. Edison. (1880, Jan. 27). Patent US223898A

[2] S. Nakamura, M. Senoh, N. Iwasa, S-I. Nagahima, “High-Brightness InGaN Blue, Green and Yellow Light-Emitting Diodes with Quantum Well Structures,” *Japanese Journal of Applied Physics,* vol. 34, no. 7A, L797-L799, 1995.

[3] I. Akasaki, H. Amano, “Crystal growth and conductivity control of group III nitride semiconductors and their application to short wavelength light emitters,” *Japanese Journal of Applied Physics*, vol. 36, no. 9R, 5393-5408, 1997.

[4] I. Akasaki, H. Amano, S. Nakamura, “Blue LEDs – filling the world with new light,” *The Royal Swedish Academy of Sciences-The Nobel Prize of Physics*, 2014.

[5] Council of European Union. “Commission Regulation (EC) No 244/2009 of 18 March 2009 implementing Directive 2005/32/EC of the European Parliament and of the Council with regard to ecodesign requirements for non-directional household lamps.” 2009.

[6] G. Zissis, P. Bertoldi, T. Serrenho, “Update on the Status of LED-Lighting world market since 2018”, Technical report, *Publications Office of the European Union*, Luxembourg, 2021.

[7] G. Perino, T. Pioch, “Banning incandescent light bulbs in the shadow of the EU emissions trading scheme,” *Climate Policy*, vol. 17, no. 5, 678-686, 2017.

[8] N. Howarth, J. Rosenow, “Banning the bulb: Institutional evolution and the phased ban of incandescent lighting in Germany,” *Energy Policy*, vol. 67, 737-746, 2014.

[9] IEEE Power Electronics Society, “IEEE recommended practices for modulating current in high-brightness LEDs for mitigating health risks to viewers”, IEEE Standard 1789-2015, *The Institute of Electrical and Electronics Engineers*, 2015.

[10] International Commission on Illumination (CIE), “CIE TN 006:2016. “Visual Aspects of Time-Modulated Lighting Systems – Definitions and Measurement Models”, Technical Note, *Commission Internationale de l’Éclairage*, Vienna, AT, 2016.

[11] A. Wilkings, J. Weitch, B. Lehman, “LED lighting flicker and potential health concerns: IEEE standards PAR 1789 update,” *Energy Conversion Congress and Exposition (ECCE)*, Atlanta, GA, pp. 171-178, 2010.

[12] A. Okumura, K. Aso, T. Ishikawa, “Follow-up survey on seizures induced by animated cartoon TV program ‘Pocket Monster,’” *Epilepsia,* vol. 45, no. 4, 377-383, 2004.

[13] International Commission on Illumination (CIE), “CIE TN 012:2021. Guidance on the Measurement of Temporal Light Modulation of Light Sources and Lighting Systems”, Technical Note, *Commission Internationale de l’Éclairage,* Vienna, AT, 2021.

[14] D. Kelly, “Visual Responses to Time-Dependent Stimuli.* I. Amplitude Sensitivity Measurements”, *Journal of the Optical Society of America*, vol. 51, no. 4, 422–429, 1961.

[15] J. Tan, N. Miller, M. Royer, L. Irvin, “Temporal light modulation: A phantom array visibility measure”, *Lighting Research & Technology*, vol. 56, no. 7, 772-789, 2024, doi:10.1177/14771535241239611

[16] European Commission, Directorate-General for Energy. “Commission Regulation (EU) 2019/2020 of 1 October 2019 laying down ecodesign requirements for light sources and separate control gears pursuant to Directive 2009/125/EC of the European Parliament and of the Council and repealing Commission Regulations (EC) No 244/2009, (EC) No 245/2009 and (EU) No 1194/2012”, 2019.

[17] R. Nordlund, V. Mantela, “Aalto implementations for flickermeter and SVM meter” [Online database], https://github.com/MantelV/Aalto-implementations-for-flickermeter-and-SVM-meter, Retrieved 30th April 2025 from DOI: https://doi.org/10.5281/zenodo.8380929.

[18] International Electrotechnical Commission (IEC), “IEC TR 61547-1:2020. Equipment for general lighting purposes – EMC immunity requirements – Part 1: Objective light flickermeter and voltage fluctuation immunity test method”, Ed. 3.0., Standard, *International Electrotechnical Commission*, Geneva, CH, 2020

[19] International Electrotechnical Commission (IEC), “IEC TR 63158:2018. Equipment for general lighting purposes – objective test method for stroboscopic effects of lighting equipment”, Ed. 1.0., Standard, *International Electrotechnical Commission*, Geneva, CH, 2018.

[20] K. Banerjee, “Light flicker assessment toolbox”, (https://www.mathworks.com/matlabcentral/fileexchange/63445-light-flicker-assessment-toolbox), *MATLAB Central File Exchange*. Retrieved March 27, 2025.

[21] V. Mantela, R. Nordlund, J. Askola, P. Kärhä, and E. Ikonen, “Novel Implementations of Digital Meters for Flicker and Stroboscopic Effect”,

Abstracts of the CIE Symposium on the Measurement of Temporal Light Modulation, October 2022, National Technical University of Athens, Greece, pp.16-17.

[22] R. Koch, and R. Zuber. "Anti-aliasing filter effects on sampling frequency and effects of mathematical implementation", in *Proceedings of the CIE Symposium on Advances on the Measurement of Temporal Light Modulation*, October 2022, National Technical University of Athens, Greece, pp. 46-53, DOI 10.25039/x49.2022.P10.

[23] C. Dam-Hansen, S. Coyne, G. Isoardi, Y. Ohno, "Minimising the uncertainties in the calculation of stroboscopic effect visibility measure," in *Proceedings of the CIE Symposium on Advances on the Measurement of Temporal Light Modulation*, October 2022, National Technical University of Athens, Greece, pp. 54-62, DOI 10.25039/x49.2022.P11.

[24] J. Drápela, J. Šlezingr, "A Light-flickermeter–Part I: Design", in *Proceedings of the 11th International Scientific Conference Electric Power Engineering* 2010, pp. 453–458, 2010.

[25] W. Mombauer, "Calculating a new reference point for the IEC-flickermeter", *European Transactions on Electrical Power*, vol. 8, no. 6, 429–436, 1998.

[26] International Electrotechnical Commission (IEC), "Testing and measurement techniques – Flickermeter – Functional and design specifications," IEC 61000-4-15, Ed. 2.0. *International Electrotechnical Commission*, 2010.

[27] S. Halpin, R. Bergeron, T. Blooming, R. Burch, L. Conrad, T. Key, "Voltage and lamp flicker issues: Should the IEEE adopt the IEC approach*?"*, *IEEE Transactions on Power Delivery*, vol. 18, no. 3, 1088–1097, 2003.

[28] A.V Oppenheim, R.W. Shafer, *Discrete-Time Signal Processing*. 3rd Edition. Prentice Hall, 2010.

[29] F. Harris, "On the use of windows for harmonic analysis with the discrete Fourier transform", *Proceedings of the IEEE*, vol. 66, no.1, 51-83, 1978.

[30] International Commission on Illumination (CIE), "CIE TN 012:2021. Guidance on the Measurement of Temporal Light Modulation of Light Sources and Lighting Systems," Technical Note, *Comission Internationale de l'Éclairage*, Vienna, AT, 2021.

[31] M. Perz, I. Vogels, D. Sekulovski, L. Wang, Y. Tu, I. Heyendrickx, "Modelling the visibility of the stroboscopic effect occurring in temporally modulated light systems," *Lighting Research & Technology*, vol. 47, no. 3, 281-300, 2014.

[32] Bureau International des Poids et Mesures, "General Conference on Weights and Measures: Proceedings of the 26th CGPM (2018)," 2019.

[33] International Commission on Illumination (CIE), "The basis of physical photometry," technical report, *Comission Internationale de l'Éclairage,* 1983.

[34] Chroma USA, *Chroma 61600 series datasheet* [Online]. Available: https://www.chromausa.com/pdf/61600%20Low%20Power%20Programmable%20AC%20Source%20022024.pdf (Accessed March 26th, 2025)

[35] R. Nordlund, "Validation for measurement of Temporal Light Artefacts on LED light sources," M.Sc. Thesis, Aalto University, Finland, 2022.

[36] C. Martinsons, N. Picard, "Untangling light in noisy luminous environments," *Lighting Research & Technology*, OnlineFirst, 2024. doi:10.1177/14771535241266178.

[37] C. Schrader, S. Pendsa, J. Ledig, "Assessment of spatially resolved temporal light modulation in extended scenes by fast imaging measurements", *Measurement Science and Technology*, vol. 36, 025902, 2025.

[38] Senop Oy, *Senop HSC-2 brochure* [Online]. Available: https://senop.fi/wp-content/uploads/senop-hsc-2-hyperspectral-camera-V3iAWSvw.pdf (Accessed April 7th, 2025)

[39] X. Xu, A. Collin, S. Djokic, R. Langella, A. Testa, J. Drapela, "Experimental evaluation and classification of LED lamps for typical residental applications", in *2017 IEEE PES Innovative Smart Grid Technologies Conference Europe (ISGT-Europe)*, pp. 1-6, IEEE, 2017.

[40] J. Drapela, R. Langella, A. Testa, A.J. Collin, X. Xu, S.Z. Djokic, "Experimental evaluation of classification of LED lamps for light flicker sensitivity," in *2018 18th International Conference on Harmonics and Quality of Power (ICHQP)*, pp. 1-6, IEEE, 2018.

[41] C. Branas, F.J. Azcondo, J.M. Alonso, "Solid-state lighting: A system review," *IEEE Industrial Electronics Magazine*, vol. 7, no. 4, 6-14, 2013.

[42] G. Udny Yule, *An Introduction to the Theory of Statistics*, pp.147-148, 14th Edition, Charles Griffin & Co LTD, 1958.

[43] S. Ross, *Introductory statistics*. pp. 90-91 and 103-104, 3rd Edition, Elsevier, 2010.

[44] U. Graham, I. Cook, *Understanding Statistics,* pp. 55-56, Oxford University Press, 1996.

[45] European Union. *European Product Registry for Energy Labelling,* [Online database], Retrieved 9 July 2024 from https://eprel.ec.europa.eu/screen/product/lightsources (Accessed April 25th, 2025)

Business, Economy
Art, Design, Architecture
Science, Technology
Crossover
Doctoral Theses

Aalto DT 164/2025

ISBN 978-952-64-2699-0
ISBN 978-952-64-2698-3 (pdf)

Aalto University
School of Electrical Engineering
Department of Electrical Engineering and Automation
aalto.fi